

Vortex localization in single crystals of $\text{Tl}_2\text{Ba}_2\text{CuO}_{6+\delta}$ with columnar defects

E. R. Nowak, S. Anders, and H. M. Jaeger

The James Franck Institute and Department of Physics, The University of Chicago, Chicago, Illinois 60637

J. A. Fendrich, W. K. Kwok, R. Mogilevsky, and D. G. Hinks

Materials Science Division, Argonne National Laboratory, Argonne, Illinois 60439

(Received 21 August 1996)

We investigate the effect of columnar defects on the low-temperature magnetic response of a highly anisotropic superconductor. Using a *local* magnetic field sensor, the vortex creep rate in single crystals of $\text{Tl}_2\text{Ba}_2\text{CuO}_{6+\delta}$ containing columnar defects is found to be a highly nonmonotonic function of vortex density. The creep rate is largest when the vortex density is less than the defect density. A strong suppression of the creep rate is observed near the matching field, B_ϕ , corresponding to equal numbers of vortices and defects. We tentatively associate this finding with the Mott-insulator line phase proposed by Nelson and Vinokur [Phys. Rev. B **48**, 13 060 (1993)]. For higher vortex densities, an additional minimum is found near $3B_\phi$, emphasizing the importance of vortex interactions. [S0163-1829(96)50542-4]

The rich magnetic phase diagrams that describe the mixed state of the cuprate high-temperature superconductors are a consequence of thermal fluctuations and disorder which strongly affect the statics and dynamics of flux-line vortices.¹ Extended defects, in particular, serve as strong pinning centers for vortices aligned along their direction. Such correlated disorder has been shown to significantly shift the irreversibility line, and thus the onset of dissipation, to higher temperatures and fields.² At low temperatures, a phase transition to a Bose-glass phase with vortex lines localized on the defects is predicted to occur from a liquid of delocalized vortex lines.³ Of profound technological and scientific potential, the Bose-glass phase is readily accessible experimentally through the controlled introduction of columnar defects. These defects are obtained by heavy-ion irradiation and consist of randomly distributed, linear tracks of damaged material extending through the sample. Buried in the Bose-glass phase for fields near $B=B_\phi$ is the postulated Mott-insulator line phase;³ B_ϕ is the matching field for which, on average, each columnar defect is occupied by one vortex. In this regime, vortices are localized by both defects and interactions with neighboring vortices. Moreover, the vortex assembly is predicted to be incompressible; the vortex density remains locked at the density of defects over a finite range of external fields. The existence of such a phase is supported by recent experiments that show a deep minimum in the field dependence of the vortex creep rate near the matching field in untwinned $\text{YBa}_2\text{Cu}_3\text{O}_{7-\delta}$ (YBCO) single crystals,⁴ and by magnetization experiments in superconducting Pb/Ge multilayer films containing a regular array of submicron holes.⁵

A potentially very different situation exists in the highly anisotropic Tl- and Bi-based compounds. Here, weak Josephson coupling between adjacent CuO_2 layers leads to a two dimensional (2D) ‘‘pancake’’ description⁶ of vortices as opposed to the 3D line objects that exist in YBCO. At high temperatures, experiments in samples of $\text{Bi}_2\text{Sr}_2\text{CaCu}_2\text{O}_{8+\delta}$ single crystals⁷ and $\text{Tl}_2\text{Ba}_2\text{CaCu}_2\text{O}_8$ epitaxial films⁸ containing columnar defects are nevertheless consistent with the

Bose-glass theory. These results show that vortices act as well-coupled lines for fields up to B_ϕ and indicate that columnar defects help overcome the effects of material anisotropy. However, as temperature is decreased the distinguishing features produced by columnar defects become less pronounced.^{2,7,8} At low temperatures in highly anisotropic systems the role of columnar defects is still unexplored.

In this paper we address this issue by investigating the magnetic response in single crystals of the anisotropic superconductor $\text{Tl}_2\text{Ba}_2\text{CuO}_{6+\delta}$ (Tl-2201) containing columnar defects. We present systematic measurements of the *local* magnetization and its time decay at temperatures below 12 K. At low vortex densities, $B \ll B_\phi$, we observe a considerable enhancement in both critical current and decay rate which is followed by a sharp suppression in the decay rate at $B \approx B_\phi$ where all vortices become locked onto defects. A second minimum in the decay rate is observed at $B \approx 3B_\phi$, resulting from a combination of defect pinning and vortex interactions. As a function of temperature, these features are found to persist well into the thermally activated regime. We interpret the behavior at $B=B_\phi$ as evidence for the predicted Mott-insulator line phase within the Bose glass.

Single crystals of Tl-2201 were synthesized using the flux-growth method at 1000 °C and 1200 psi Ar pressure, as described in detail elsewhere.⁹ The two samples we studied were made under identical conditions and were irregularly shaped platelets with basal plane areas approximately $(200 \mu\text{m})^2$ and 20- μm thick along the *c* axis. Randomly distributed columnar defects aligned along the *c* axis ($\pm 2^\circ$) were introduced by irradiating one of the crystals with 1.1 GeV uranium ions at the ATLAS source. The large ionization energy loss ($> 2.5 \text{ keV}/\text{\AA}$) of these ions across the thickness of the sample ensured the formation of linear tracks of amorphous material. The irradiation dosage was chosen so that the density of defects corresponded to vortex densities at a matching field $B_\phi = 10 \text{ kG}$. After irradiation, the transition temperature T_c , was suppressed from ~ 87 to $\sim 78 \text{ K}$.

Magnetization measurements were performed using microfabricated bismuth Gaussmeters, similar to those used in

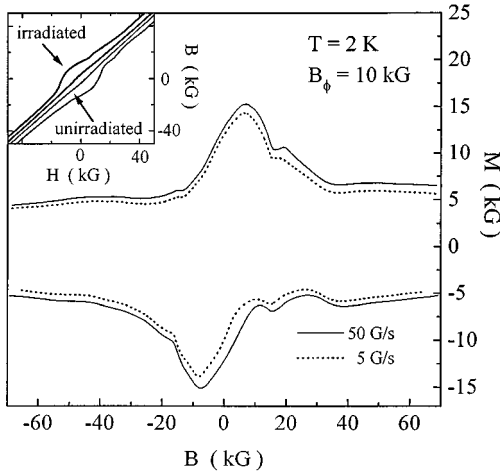


FIG. 1. Magnetization, M , vs local internal field, B , at $T=2$ K for the crystal with a columnar defect density corresponding to a vortex density at a field $B_\phi = 10$ kG. The hysteresis loop is narrower for slower sweep rates of the applied field. Data shown in subsequent figures correspond to the lower right-hand quadrant. Inset: columnar defects enlarge the hysteresis loop, particularly for $|B| < B_\phi$.

Ref. 4 over a range of temperatures, $0.4 \leq T \leq 12$ K, and for applied magnetic fields, $-80 \leq H \leq 80$ kG, along the direction of irradiation. The magnetic field penetrating the $(3 \mu\text{m})^2$ active area of the probe was detected by the induced Hall voltage. The probe was calibrated over the full range of temperatures and applied fields used in the experiment. This calibration curve is a monotonically increasing function of H : it is weakly cubic in H for $|H| < 1$ T, and nearly linear in H above 1 T. The crystals were then mounted directly onto the Gaussmeters using a thin layer of vacuum grease; we estimate the sample to probe separation to be about $1 \mu\text{m}$. All data were recorded after the applied field was swept through a sufficiently large range (~ 40 kG) to ensure that a well-defined gradient in the vortex density was established throughout the sample.

The presence of columnar defects affects the shape of the hysteresis loop, $B(H)$, and magnetization curve, $M(B)$, shown in Fig. 1. We define the *local* magnetization of the sample as $M = B - H$, where B is the local, internal field in the crystal at the Gaussmeter's position. It has recently been postulated¹⁰ and shown⁴ that columnar defects lead to two critical current regimes as a function of internal field: an enhanced critical current in regions of the sample where $B < B_\phi$ for which each vortex is strongly pinned by a columnar defect, and a smaller critical current in regions where $B > B_\phi$ due to interstitial vortices that are less strongly pinned by point disorder and/or vortex interactions. The larger critical current is reflected by the central bulge in the hysteresis loop and the appearance of a peak in $M(B)$ near $|B| = 8$ kG for both increasing and decreasing field in Fig. 1. The inset of Fig. 3 illustrates how, for $B < B_\phi$, a steeper vortex density gradient (corresponding to the larger critical current) leads to a peak in the local magnetization. A double-sloped vortex density gradient means that the Bean model¹¹ cannot be used to estimate the critical current density, J_c .

The values of the magnetization are not the same for fields applied in the positive and negative directions (Fig. 1).

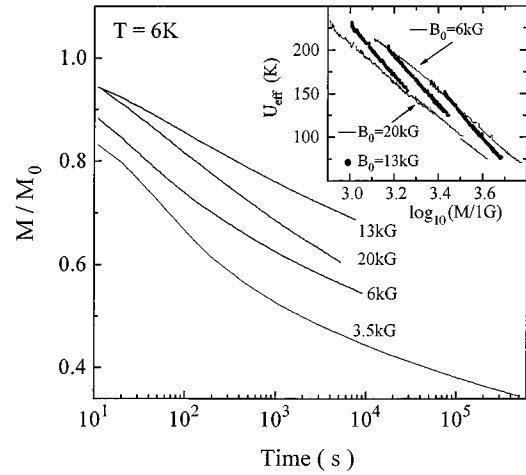


FIG. 2. Time decay of the magnetization measured at $T=6$ K for the irradiated crystal. Significant decay occurs and is typically nonlogarithmic, especially for $|B| < B_\phi$. Curves are normalized according to the initial magnetization, M_0 , and internal field, B_0 , measured at an applied field sweep rate of 50 G/s. Inset: effective energy barrier for flux creep, U_{eff} , vs local magnetization at selected B_0 .

We note that demagnetization effects from the sample introduce a radial component of the field at the Hall probe which cannot be calibrated, and results in a small magnetoresistive response that is an even function of field. This may account for asymmetries of the measured local field, its gradient, and the magnetic relaxation rate (see below) with respect to the applied field that we and others^{4,12} have observed. Asymmetries can be minimized by positioning and local field probe at the center of a regularly shaped crystal.⁴

The magnetization decay at different internal fields is shown in Fig. 2 for $T=6$ K. The time dependence is typically nonlogarithmic which we attribute to two factors: a nonlinear current dependence of the effective pinning barrier to vortex motion,¹³ $U_{\text{eff}}(J)$, and the strong dependence of the decay rate on the local, internal field which we discuss below. For this reason, only the initial stage of the magnetic relaxation (10–1000 s) was used to calculate the normalized decay rate, $S(B, T) \equiv (1/M_0) dM/d \ln(t)$; M_0 is the initial magnetization taken from the M vs B curve for a ramp rate of 50 G/s. The decay rate, S calculated at positive internal fields and negative magnetizations (see Fig. 1), shows rapid and nonmonotonic variations as a function of *local* internal field, as shown in Fig. 3 by the symbols. We note that the S vs B curve can also be asymmetric for increasing and decreasing field branches. In this case, symmetry is not expected since the vortex density profile inside the sample differs significantly for flux entry and flux exit as shown in the inset to Fig. 3.

The minima in the decay rate at $B \approx B_\phi$ and $B \approx 3B_\phi$ seen in Fig. 3 are robust. We have explicitly verified that fitting the magnetization decay to interpolation and power-law forms¹ over the entire length of the relaxation data record (typically over 10^4 s) does not affect the position of the minima in $S(B)$. The error in the fits is approximately the size of the data symbols in Fig. 3. Because the size of the hysteresis loop depends on the rate at which the applied field is ramped, we can furthermore compare S with a dynamical

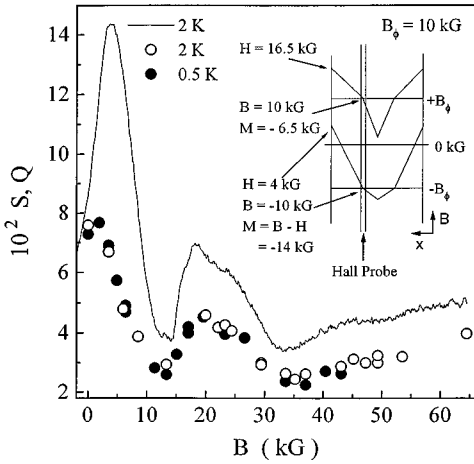


FIG. 3. Magnetization decay rates show sharp minima for internal fields near B_ϕ and $3B_\phi$. Symbols represent rate, S , determined with the applied field held constant. Solid line shows the dynamical rate, Q , calculated from the sweep rate dependence of the hysteresis loop. Inset: a model incorporating two critical currents in irradiated crystals can explain the maxima in the magnetization (Fig. 1) as the applied field is ramped up from large negative to large positive values.

magnetization decay rate,¹⁴ $Q(B) \equiv \ln[M_f(B)/M_s(B)] / \ln(\Omega_f/\Omega_s)$. $Q(B)$ is obtained from magnetization data, $M_{f,s}$, taken at two different rates: a fast ramp rate Ω_f and a slower rate Ω_s . This technique gives a continuous curve for $Q(B)$, as compared to the discrete set of values for $S(B)$ which are obtained from individual relaxation traces (Fig. 2). The solid line in Fig. 3 shows $Q(B)$ calculated from ramp rates of 50 and 5 G/s. Although quantitative differences exist, partly due to nonlogarithmic decay over the respective time windows for which the quantities were calculated, the variations with field are in excellent agreement with $S(B)$.

The sharp suppression in the decay rate and the local maximum in the magnetization at $B \approx B_\phi$ signify a developing rigidity of the glassy vortex configuration as vortices become localized. The sharp minimum in S can be interpreted as a gap opening up in the excitation spectrum¹⁵ which effectively deepens the potential wells and inhibits vortex motion at the matching field. We take this as strong evidence for the Mott-insulator line phase in this anisotropic material. By comparison, measurements of the unirradiated sample showed a roughly field-independent decay rate, $S(T=2 \text{ K}) = 0.033 \pm 0.005$. The nonvanishing decay rate at $B \approx B_\phi$ for the irradiated crystal is at least partly due to the finite size of the Hall probe and vortex density gradients in the crystal that prevent all vortices from being localized on defects at the same time. Likewise, vortex flow in different parts of the crystal may affect the decay rate at the position of the Hall probe. This may explain why the minimum in S is found at $1.2B_\phi$ and not B_ϕ . Also, positional disorder in the columnar defects will occasionally result in two closely spaced defects.¹⁵ In this case, and for $B \approx B_\phi$, repulsion between vortices will force one of the vortices to leave its defect and move to an interstitial site where it is less strongly pinned. A slightly increase in field (vortex density) may then be necessary to optimally localize these interstitial vortices by interactions with vortices trapped on the defects.

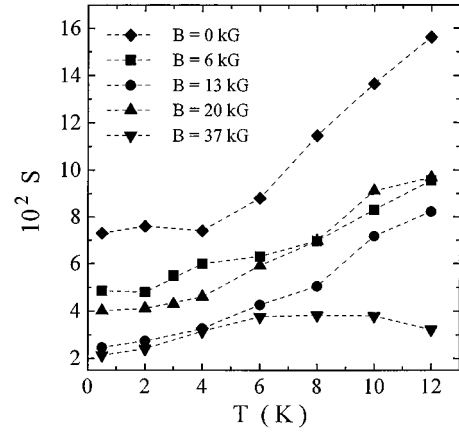


FIG. 4. Temperature dependence of S for the irradiated crystal, $B_\phi = 10 \text{ kG}$, at several internal fields, B . The nonmonotonic behavior of the decay rate shown in Fig. 3 is apparent out to $T = 12 \text{ K}$.

The temperature dependence of the decay rate for selected values of B is shown in Fig. 4. For $T < 4 \text{ K}$, S is found to be finite and nearly temperature independent (see also Fig. 3); this may suggest that vortex motion is not thermally activated but occurs by quantum tunneling.^{4,16} If so, Fig. 4 indicates that the nonmonotonic behavior in $S(B)$, and thus presumably the Mott-insulator phase, survives the crossover from quantum tunneling to thermal activation at higher temperatures, at least up to $T = 12 \text{ K}$.

We have repeated the procedure given by Maley *et al.*¹³ with our data between 6 and 12 K to obtain the field dependence of the pinning barrier $U_{\text{eff}}(B, M)$ from relaxation curves taken at different temperatures¹⁷ (see Fig. 2, inset). The slopes of the resulting isothermal segments are proportional to the characteristic energy barrier, U_0 . We note that with two critical current regions in the crystal, the usual assumption¹¹ that $M \propto J$ is a poor approximation, especially near B_ϕ , where J is considerably underestimated.¹⁸ Nevertheless, fits of our data to the functional forms proposed by collective creep theory,¹⁹ the Bose-glass model,³ as well as that observed by Zeldov *et al.*^{13,20} do not yield the expected¹ monotonic dependence of U_0 on B . Instead, we find that U_0 is largest at $B \approx B_\phi$ which is consistent with the minimum in S at the matching field (Fig. 3). Moreover, this analysis indicates that the nonlinear current dependence to the pinning potential is particularly strong at the matching field, and thus may reflect a property of the Mott-insulator phase.

We attribute the large decay rates and the modest reduction of S at $B \approx B_\phi$ (by a factor of 4, compared to a factor ≥ 10 in irradiated, untwinned YBCO crystals),⁴ to a small flux line tension. Brandt⁶ has shown that for the Bi- and Tl-based compounds the large anisotropy ratio, $\Gamma = \lambda_c/\lambda_{ab} \sim 50$ ($\Gamma \approx 5$ for YBCO), reduces the line tension ($\propto \Gamma^{-2}$) of a flux line, thereby leading to the thermal depinning of vortex segments that are smaller than the CuO_2 layer spacing; that is, pancake vortices in the CuO_2 layers can depin individually. This leads to large decay rates even at low temperatures.

Although irradiated YBCO crystals do show a pronounced minimum in S at $B \approx B_\phi$, no additional dip is seen for $B > B_\phi$; instead, S is found to asymptotically approach the behavior for point-defect dominated pinning.⁴ For suffi-

ciently strong vortex interactions, i.e., large enough elastic energies of the vortex arrangement, the formation of locally ordered regions will compete with the randomness in the defect positions. An additional minimum in $S(B)$ and an associated peak in the magnetization at $B = 3B_\phi$ would, indeed, be expected for a triangular lattice of columnar defects with density B_ϕ , in which interstitial vortices are caged in by the repulsive interactions with their six nearest neighbors. Our observations of such features at this second matching field suggest that despite positional disorder of the columnar defects, pinned (distorted) triangular vortex arrangements survive locally and can be detected by local measurements. Different vortex configurations or completely random arrangements would lead to different matching fields or their complete absence; for a square lattice of columnar defects the second matching field would occur at $B \approx 2B_\phi$, as seen by Baert *et al.*⁵ Furthermore, point disorder must be a comparatively weak perturbation on this vortex-vortex interaction barrier which cages interstitial vortices. Presumably, the small flux line tension in anisotropic superconductors prevents point disorder from collectively pinning a long segment of an interstitial flux line and thereby leading to random spatial arrangements. Within this picture, the increase in S at intermediate fields and for $B > 3B_\phi$ in Fig. 3 naturally arises from interstitial vortices which are less strongly pinned and find it easier to escape out of irregular confining cages consisting of five or seven vortices.

It is interesting to speculate whether the features at $3B_\phi$ are a manifestation of a Mott-insulator behavior in the

weakly pinned Bose-glass phase proposed in Ref. 10 for $B > B_\phi$. Since interstitial vortices are expected to be pinned less strongly, it is surprising to find the decay rate near $3B_\phi$ to be as low and to have a weaker temperature dependence than that near B_ϕ . This observation requires further study. Finally, we note that for $B < B_\phi$, both the vortex creep rate and the critical current are enhanced when compared to the unirradiated crystal (at least over the measured range of temperatures); this is contrary to the classical Anderson-Kim description,²¹ where $S \propto 1/U_0$ and $J_c \propto U_0$. Here, U_0 is the pinning energy which presumably is increased by the introduction of columnar defects.

While the original work on boson localization²² cannot account for a Mott-insulator phase on a disordered lattice such as that formed by columnar defects, the existence of this phase within the Bose-glass was postulated by Nelson and Vinokur.³ We believe that our results provide evidence of this phase in an anisotropic vortex system and hope they motivate further theoretical investigation.

We gratefully acknowledge the assistance of B. Glagola with the heavy-ion irradiation and of K. Zhang with the Laue x-ray diffraction measurements. We thank K. M. Beauchamp, L. Radzihovsky, T. F. Rosenbaum, and E. Shung for enlightening discussions. This work was supported by the National Science Foundation (Grant No. DMR91-20000) through the Science and Technology Center for Superconductivity. W.K.K. and D.G.H. acknowledge support from the DOE, Basic Energy Sciences-Materials Science, under Contract No. W-31-109-ENG-38.

-
- ¹G. Blatter *et al.*, Rev. Mod. Phys. **66**, 1125 (1994), and references therein.
- ²L. Civale *et al.*, Phys. Rev. Lett. **67**, 648 (1991).
- ³D. R. Nelson and V. M. Vinokur, Phys. Rev. B **48**, 13 060 (1993).
- ⁴K. M. Beauchamp *et al.*, Phys. Rev. Lett. **75**, 3942 (1995); Phys. Rev. B **52**, 13 025 (1995).
- ⁵M. Baert *et al.*, Phys. Rev. Lett. **74**, 3269 (1995).
- ⁶J. R. Clem, Phys. Rev. B **43**, 7837 (1991); E. H. Brandt, Europhys. Lett. **18**, 635 (1992).
- ⁷C. J. van der Beek *et al.*, Phys. Rev. Lett. **74**, 1214 (1995).
- ⁸R. C. Budhani, W. L. Holstein, and M. Suenaga, Phys. Rev. Lett. **72**, 566 (1994).
- ⁹R. Mogilevsky and D. G. Hinks (unpublished).
- ¹⁰L. Radzihovsky, Phys. Rev. Lett. **74**, 4923 (1995); **74**, 4919 (1995).
- ¹¹C. P. Bean, Phys. Rev. Lett. **8**, 250 (1962).
- ¹²D. A. Brawner, N. P. Ong, and Z. Z. Wang, Nature (London) **358**, 567 (1992).
- ¹³M. P. Maley *et al.*, Phys. Rev. B **42**, 2639 (1990); E. Zeldov *et al.*, Appl. Phys. Lett. **56**, 680 (1990).
- ¹⁴M. Jirsa *et al.*, Physica C **207**, 85 (1993).
- ¹⁵U. C. Täuber *et al.*, Phys. Rev. Lett. **74**, 5132 (1995).
- ¹⁶D. Prost *et al.*, Phys. Rev. B **47**, 3457 (1993).
- ¹⁷E. R. Nowak, S. Anders, and H. M. Jaeger (unpublished).
- ¹⁸A single critical current throughout the crystal is expected when $B \approx 0$ or $B > 20$ kG. In this case, $M \propto J$ is a better approximation. Thus, the isothermal segments for $B = 13$ kG $\approx B_\phi$ (Fig. 2, inset) are shifted to lower currents (smaller M) and their slopes are reduced. This may also account for why these segments, unlike those for $B \neq B_\phi$, do not assemble to form a continuous curve.
- ¹⁹M. V. Feigel'man *et al.*, Phys. Rev. Lett. **63**, 2303 (1989).
- ²⁰Y. Yeshurun and A. P. Malozemoff, Phys. Rev. Lett. **60**, 2202 (1988).
- ²¹P. W. Anderson and Y. B. Kim, Rev. Mod. Phys. **36**, 39 (1964).
- ²²M. P. A. Fisher *et al.*, Phys. Rev. B **40**, 546 (1989).